

Observable ΔN_{eff} in Dirac Scotogenic Model

Debasish Borah,^{1,*} Pritam Das,^{1,†} and Dibyendu Nanda^{2,‡}

¹*Department of Physics, Indian Institute of Technology, Guwahati, Assam 781039, India*

²*School of Physics, Korea Institute for Advanced Study, Seoul 02455, South Korea*

Abstract

We study the possibility of probing the radiative Dirac seesaw model with dark sector particles going inside the loop, popularly referred to as the Dirac scotogenic model via measurements of effective relativistic degrees of freedom ΔN_{eff} at cosmic microwave background (CMB) experiments. The loop suppression and additional free parameters involved in neutrino mass generation allow large ($\sim \mathcal{O}(1)$) coupling of light Dirac neutrinos with the dark sector particles. Such large Yukawa coupling not only dictates the relic abundance of heavy fermion singlet dark matter but also can lead to the thermalisation of the right chiral part of Dirac neutrinos, generating additional relativistic degrees of freedom ΔN_{eff} . We find that the parameter space consistent with dark matter phenomenology and neutrino mass bounds can also be probed at future cosmic microwave background experiments like CMB-S4 via precision measurements of ΔN_{eff} . The same parameter space, while leading to loop-suppressed direct detection cross-section of dark matter outside future sensitivities, can also have other interesting and complementary observational prospects via charged lepton flavour violation and collider signatures.

*Electronic address: dborah@iitg.ac.in

†Electronic address: prtmdas9@iitg.ac.in

‡Electronic address: dnanda@kias.re.kr

I. INTRODUCTION

Evidence from astrophysics and cosmology-based observations suggests that approximately 26% of our present universe is made up of dark matter (DM) [1, 2]. Assuming a particle origin of DM, it is also known that none of the standard model (SM) particles can give rise to DM, leading to several beyond the standard model (BSM) proposals. Among such proposals, the weakly interacting massive particle (WIMP) paradigm has been the most well-studied one for several decades. A recent review on the status of WIMP-type DM models can be found in [3]. While the primary reason for the popularity of WIMP has been its promising detection prospects, the null results at direct detection experiments [4] have pushed several simplified models to tiny corners or even motivated the particle physics community to look for alternatives beyond the WIMP paradigm. While it is premature to consider the WIMP paradigm to be ruled out, it is important to look for complementary signatures of those classes of WIMP whose direct detection prospects remain low.

The origin of neutrino mass and mixing is another motivation for pursuing BSM physics. While DM and neutrino mass could have completely different origins, it is motivating to study minimal frameworks which can relate their origins. The scotogenic model [5] provides such an arena where non-zero neutrino masses arise at a one-loop level with dark sector particles participating in the loop. While the conventional neutrino mass models, including the original scotogenic model, predict Majorana light neutrinos, there is no experimental evidence of light neutrinos being of Majorana type. This has also led to some interest in the origin of light Dirac neutrino mass of sub-eV scale. Assuming a global unbroken lepton number symmetry, this can be minimally achieved in the SM just by incorporating three gauge singlet right-handed (RH) neutrinos, which couple to the left-handed neutrinos via the SM Higgs doublet with a tiny Yukawa coupling of the order $\lesssim 10^{-12}$. A possible extension of this minimal setup can naturally explain the smallness of light Dirac neutrino mass while also solving the puzzle of DM at the same time. In this work, we consider such a WIMP DM scenario which is not only connected to the origin of light neutrino masses, another observed phenomenon that the SM fails to address, but can also have complementary cosmological probes. In particular, we consider light neutrinos to be of Dirac nature whose sub-eV mass arises at one-loop, in a way similar to the scotogenic mechanism [5] originally put forward for Majorana light neutrinos. The heavy scalar and fermionic fields going inside the loop

are stabilized by an unbroken Z_2 symmetry such that the lightest Z_2 -odd particle can be a DM candidate. We consider the extension of this model to light Dirac neutrinos. If Z_2 -odd fermion singlet is considered to be WIMP DM, it will thermalize via Yukawa interactions leading to the thermalization of light Dirac neutrinos simultaneously. Since Dirac neutrino also contains the right chiral part, its thermalization can lead to additional relativistic degrees of freedom or dark radiation, which can be probed in cosmic microwave background (CMB) experiments. Existing CMB constraints put limits on effective degrees of freedom for neutrinos during the era of recombination ($z \sim 1100$) as [2]

$$N_{\text{eff}} = 2.99^{+0.34}_{-0.33} \quad (1)$$

at 2σ or 95% CL including baryon acoustic oscillation (BAO) data, which becomes more stringent to $N_{\text{eff}} = 2.99 \pm 0.17$ at 1σ CL. A similar bound also exists from big bang nucleosynthesis (BBN) $2.3 < N_{\text{eff}} < 3.4$ at 95% CL [6]. While these bounds are consistent with SM predictions $N_{\text{eff}}^{\text{SM}} = 3.045$ [7–9] (the recent calculation suggests a smaller value as $N_{\text{eff}}^{\text{SM}} = 3.0440 \pm 0.0002$ [10, 11]), future experiments like CMB Stage IV (CMB-S4) is expected to reach an unprecedented sensitivity of $\Delta N_{\text{eff}} = N_{\text{eff}} - N_{\text{eff}}^{\text{SM}} = \pm 0.06$ [12], taking it closer to the SM prediction. Enhancement of ΔN_{eff} in Dirac neutrino models have been studied in several recent works [13–27]. Though these works discuss the enhancement of ΔN_{eff} due to light Dirac neutrinos, this is the first time such a possibility is explored and relevant constraints are imposed in the minimal Dirac scotogenic model.

The primary motivation of this work is to find a viable correlation among light Dirac neutrino mass, DM relic abundance and cosmological observables like ΔN_{eff} while incorporating experimental bounds from colliders, lepton flavour violation (LFV) etc. While there exist a variety of radiative seesaw models [28] with low seesaw scale and observable consequences at terrestrial experiments, radiative Dirac seesaw models have the complementary detection prospects in terms of ΔN_{eff} due to the presence of additional light degrees of freedom. Moreover, the Dirac scotogenic model comes with the added advantage of explaining the origin of DM as well. This leads to the possibility of having a highly testable scenario where different observables in cosmic, energy and intensity frontiers can be dictated by the same particles and their couplings enhancing the predictivity. Starting with the most minimal version of the Dirac scotogenic model, we perform a comprehensive analysis taking all relevant constraints into account while also indicating the prospects of future experimental

discovery via CMB as well as particle physics-based experiments. We show that in this minimal Dirac scotogenic model with fermion singlet DM, a large enhancement to ΔN_{eff} can be obtained with an interesting interplay of DM phenomenology, neutrino mass with tantalizing observational prospects via charged lepton flavour violation.

This paper is organized as follows. In section II we briefly discuss the most minimal version of the Dirac scotogenic model. In section III, we discuss the details of our calculations related to DM observables, ΔN_{eff} as well as LFV. We present our results in section IV and finally conclude in section V.

II. DIRAC SCOTOGENIC MODEL

Dirac scotogenic model has been discussed in several earlier works [29–42] in different contexts and with different motivations. While some of these models have also incorporated additional gauge symmetries, we consider a minimal version requiring only the minimal fields augmented with discrete symmetries to realise the scenario. The SM is extended by three generations of right-handed neutrinos (ν_{Ri}), three vector-like fermionic singlets (N_i), one inert scalar doublet (ϕ) and one inert real scalar singlet (χ). The relevant particle content of our model is projected in table I. In addition to these new particles, a $Z_3 \times Z_2$

	L	H	ν_R	N	ϕ	χ
$SU(2)$	2	2	1	1	2	1
$U(1)_Y$	$-\frac{1}{2}$	$\frac{1}{2}$	0	0	$\frac{1}{2}$	0
Z_3	0	0	ω	ω	ω	0
Z_2	+	+	+	-	-	-

TABLE I: Particle content of the model with respective quantum numbers under the symmetry group.

symmetry, under which all the SM particles transform trivially, is imposed to forbid the tree-level Dirac neutrino mass term, the Majorana mass terms of ν_R , N and also to stabilise the DM particle (N_1). The presence of a global lepton number symmetry (under which newly introduced fermions and SM leptons carry lepton number 1) is assumed in order to forbid Majorana mass terms at higher loop levels. This choice of particles and symmetries

leads to the following Yukawa interactions

$$-\mathcal{L}_{\text{Yukawa}} \supset \left((y_\phi)_{ij} \bar{L}_i \tilde{\phi} N_j + (y_\chi)_{ij} \bar{\nu}_{Ri} N_j \chi + \text{h.c.} \right) + (M_N)_{ij} \bar{N}_i N_j \quad (2)$$

where $i, j = 1, 2, 3$ denotes three generations of fermions and $\tilde{\phi} = i\sigma^2 \phi^*$. Without loss of generality, we assume M_N to be diagonal. These Yukawa interactions will play a very crucial role in generating Dirac neutrino mass as well as DM relic abundance. The scalar potential of the model can be written as follows,

$$\begin{aligned} V = & -\mu_H^2 H^\dagger H + \mu_\phi^2 \phi^\dagger \phi + \frac{1}{2} \mu_\chi^2 \chi^2 + \frac{1}{2} \lambda_1 (H^\dagger H)^2 + \frac{1}{2} \lambda_2 (\phi^\dagger \phi)^2 + \frac{1}{4!} \lambda_3 \chi^4 \\ & + \lambda_4 (H^\dagger H)(\phi^\dagger \phi) + \frac{1}{2} \lambda_5 (H^\dagger H) \chi^2 + \frac{1}{2} \lambda_6 (\phi^\dagger \phi) \chi^2 + \lambda_7 (H^\dagger \phi)(\phi^\dagger H) \\ & + \mu (\phi^\dagger H + H^\dagger \phi) \chi. \end{aligned} \quad (3)$$

As mentioned, we kept the singlet scalar χ as real for simplicity. This potential does preserve Z_2 symmetry while Z_3 is softly broken by the last term, which gives us the freedom to choose μ to be very small. As discussed later, this soft breaking is necessary to generate light neutrino mass at one loop. The mass spectrum for the physical scalars, after electroweak symmetry breaking, can be obtained as follows:

$$M_h^2 = 2\lambda_1 v^2; \quad (4)$$

$$M_{\phi^\pm}^2 = \mu_\phi^2 + \lambda_4 v^2; \quad (5)$$

$$M_{\phi_I}^2 = \mu_\phi^2 + (\lambda_4 + \lambda_7) v^2; \quad (6)$$

$$M_{\chi, \phi_R}^2 = \begin{pmatrix} \mu_\chi^2 + \lambda_5 v^2 & \sqrt{2} \mu v \\ \sqrt{2} \mu v & \mu_\phi^2 + (\lambda_4 + \lambda_7) v^2 \end{pmatrix}; \quad (7)$$

where v denotes the vacuum expectation value (VEV) of the neutral component of the SM Higgs doublet H . The neutral component of the Z_2 -odd scalar doublet is composed of real and complex parts ($\phi^0 = \phi_R + i\phi_I$) and the real component of ϕ mixes with χ via a mixing angle θ as shown by the mass matrix squared above. Diagonalising this gives rise to two mass eigenstates having masses M_{S_1} and M_{S_2} , which can be expressed as follows:

$$\begin{pmatrix} S_1 \\ S_2 \end{pmatrix} = \begin{pmatrix} \cos \theta & \sin \theta \\ -\sin \theta & \cos \theta \end{pmatrix} \begin{pmatrix} \chi \\ \phi_R \end{pmatrix} \quad \text{where,} \quad \theta = \tan^{-1} \left[\frac{2\sqrt{2}\mu v}{\mu_\phi^2 - \mu_\chi^2 + (\lambda_4 - \lambda_5)v^2} \right]. \quad (8)$$

The relevant free parameters are the four masses (M_{S_1} , M_{S_2} , M_{ϕ^\pm} and M_N), the quartic coupling (λ_5), mixing angle (θ) and the Yukawa couplings (y_ϕ , y_χ). They will simultaneously

impact the neutrino mass generation, thermalisation of ν_R , annihilation and co-annihilation rates of dark matter in the early universe. In the upcoming sections, we will discuss the importance of these parameters in detail.

A. Neutrino mass and LFV

As mentioned earlier, light Dirac neutrino mass can be generated at the one-loop level as shown on the left panel of Fig. 1. The one-loop Dirac neutrino mass can be estimated as [30, 39]:

$$(M_\nu)_{\alpha\beta} = \frac{\sin 2\theta}{32\pi^2\sqrt{2}} \sum_{k=1}^3 (y_\phi)_{\alpha k} (y_\chi^*)_{\beta k} M_{N_k} \times \left(\frac{M_{S_1}^2}{M_{S_1}^2 - M_{N_k}^2} \ln \frac{M_{S_1}^2}{M_{N_k}^2} - \frac{M_{S_2}^2}{M_{S_2}^2 - M_{N_k}^2} \ln \frac{M_{S_2}^2}{M_{N_k}^2} \right). \quad (9)$$

Here, M_{S_1} and M_{S_2} are the masses of the physical scalars S_1 and S_2 which are the linear combination of ϕ_R and χ . The present cosmological bound [2] on neutrino mass suggests that the sum of absolute neutrino masses should satisfy $\sum m_i < 0.12$ eV. Here, we have restricted ourselves to the region of parameter space where all the new particles, except ν_R 's, have masses $\sim \mathcal{O}(100 \text{ GeV})$. This region of parameter space is imperative to find observable ΔN_{eff} while keeping the associated Yukawa couplings within limits arising from different experimental measurements as well as perturbativity. Following Eq. (9), we can get $y_\phi y_\chi \theta < 10^{-7}$ to remain consistent with the neutrino mass bound. Depending on the choices of Yukawa couplings and mixing angle, which are consistent with this bound, we categorise our analysis into three separate cases, constituting the primary content of this work.

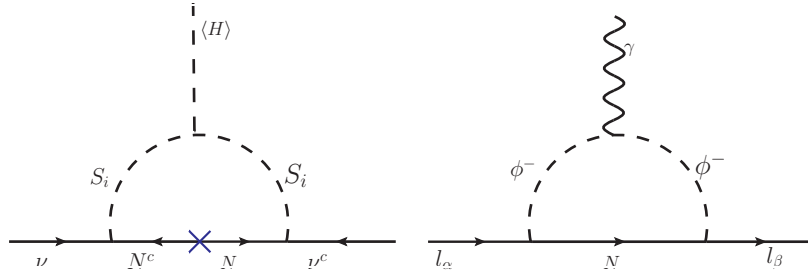


FIG. 1: *Left panel:* Neutrino mass generation at a one-loop level in Dirac scotogenic model. Here, $S_i (i = 1, 2)$ is the physical mass eigenstate. *Right panel:* one-loop contribution charged lepton flavour violating process $l_\alpha \rightarrow l_\beta \gamma$.

One interesting experimental signature of such a radiative neutrino mass model is charged lepton flavour violation. In this work, we will check the bounds from $\mu \rightarrow e\gamma$ processes only, which is tightly constrained by MEG data [43] while also having promising future sensitivity. It should be noted that such LFV decays depend crucially on the size of off-diagonal terms in y_ϕ and in our discussion, we have considered them equal to diagonal entries without loss of generality. Since only the scalar doublet (ϕ) is involved with the charged lepton interactions, only the Yukawa coupling, y_ϕ will be responsible for the decay process. The one-loop decay can arise due to the diagram shown in the right panel of Fig. 1, where l_α and l_β are the two generations of charged leptons. The effective Lagrangian for $\mu \rightarrow e\gamma$ process is given as [44]

$$\mathcal{L}_{\mu \rightarrow e\gamma} = \frac{4G_F}{\sqrt{2}} \left[m_\mu A_R \bar{\mu}_R \sigma^{\mu\nu} e_L F_{\mu\nu} + \text{h.c.} \right], \quad (10)$$

where A_R is the Wilson coefficient of the dipole operator. In this model, the expression of this coefficient is calculated as [39]

$$A_R = -\frac{\sqrt{2}}{8G_F} \frac{e(y_\phi)_{\beta i}(y_\phi^*)_{\alpha i}}{16\pi^2 M_{\phi^\pm}^2} f\left(\frac{M_{N_i}^2}{M_{\phi^\pm}^2}\right), \quad (11)$$

where the loop function is defined as

$$f(x) = \frac{1 - 6x + 2x^3 + 3x^2(1 - \ln x)}{12(1 - x)^2}. \quad (12)$$

Finally, the decay branching ratio for $\mu \rightarrow e\gamma$ is given by:

$$\text{Br}(\mu \rightarrow e\gamma) = \text{Br}(\mu \rightarrow e\nu_\mu\bar{\nu}_e) \times \frac{3\alpha_{\text{EM}}}{16\pi G_F^2} \text{Abs} \left[\sum_i \frac{(y_\phi)_{\mu i}(y_\phi^*)_{ei}}{M_{\phi^\pm}^2} f\left(\frac{M_{N_i}^2}{M_{\phi^\pm}^2}\right) \right]^2. \quad (13)$$

In the above equation, G_F is the Fermi constant and α_{EM} is the fine-structure constant. From the experimental point of view, the current upper limits on the $\mu \rightarrow e\gamma$ branching ratio from MEG-2016 result is $\text{Br}(\mu \rightarrow e\gamma) < 4.2 \times 10^{-13}$ [43], with future sensitivity being $\text{Br}(\mu \rightarrow e\gamma) < 6 \times 10^{-14}$ [45].

B. Electroweak precision tests

Due to the gauge interactions of the inert doublet ϕ and its mixing with χ , they will contribute to W^\pm and Z boson self-energies. Their contributions are often parameterised

in terms of the oblique parameters S, T and U [46, 47]. With the contribution to the U parameter being suppressed, the contribution to S and T can be written as [48, 49]

$$S = \frac{1}{\pi m_Z^2} \left[\cos^2 \theta \mathcal{B}_{22}(m_Z^2, m_{S_2}^2, m_{\phi_I}^2) + \sin^2 \theta \mathcal{B}_{22}(m_Z^2, m_{S_1}^2, m_{\phi_I}^2) - \mathcal{B}_{22}(m_Z^2, m_{\phi^+}^2, m_{\phi^+}^2) \right], \quad (14)$$

$$T = \frac{1}{16\pi^2 \alpha_{\text{em}}^2 v^2} \left[\cos^2 \theta \mathcal{F}(m_{\phi^+}^2, m_{S_2}^2) + \sin^2 \theta \mathcal{F}(m_{\phi^+}^2, m_{S_1}^2) + \mathcal{F}(m_{\phi^+}^2, m_{\phi_I}^2) - \cos^2 \theta \mathcal{F}(m_{S_2}^2, m_{\phi_I}^2) - \sin^2 \theta \mathcal{F}(m_{S_1}^2, m_{\phi_I}^2) \right], \quad (15)$$

where,

$$\mathcal{B}_{22}(q^2, m_1^2, m_2^2) = B_{22}(q^2, m_1^2, m_2^2) - B_{22}(0, m_1^2, m_2^2), \quad (16)$$

$$\mathcal{F}(x^2, y^2) = \frac{x^2 + y^2}{2} - \frac{x^2 y^2}{x^2 - y^2} \ln \left(\frac{x^2}{y^2} \right). \quad (17)$$

B_{22} is the Passarino-Veltman function [50] given by

$$B_{22}(q^2, m_1^2, m_2^2) = \frac{1}{4}(\Delta + 1)(m_1^2 + m_2^2 - \frac{1}{3}q^2) - \frac{1}{2} \int_0^1 X \ln(X - i\epsilon) dx \quad (18)$$

where,

$$X \equiv m_1^2 x + m_2^2(1-x) - q^2 x(1-x), \Delta \equiv \frac{2}{4-d} + \ln 4\pi - \gamma_E, \quad (19)$$

with d being the spacetime dimensions and $\gamma_E \sim 0.577$ being the Euler-Mascheroni constant. The current best-fit values of $S = 0.02 \pm 0.07$ and $T = 0.07 \pm 0.06$ [51] constrain the model parameter space, as we implement later in our numerical analysis.

C. Collider limits and prospects

Precision LEP data constrains the masses of inert scalar doublet ϕ components such that they do not affect the known quantities like electroweak gauge boson decay widths. For example, in order to prevent Z boson decay into the neutral components of ϕ , one must have $M_{\phi_R} + M_{\phi_I} > M_Z$. Additionally, LEP precision data also rule out the region $M_{\phi_R} < 80$ GeV, $M_{\phi_I} < 100$ GeV, $M_{\phi_I} - M_{\phi_R} > 8$ GeV [52]. A similar lower bound exists on charged scalar mass $M_{\phi^\pm} > 90$ GeV. If $M_{\phi_R, \phi_I} < M_h/2$, the large hadron collider (LHC) bound

on invisible Higgs decay comes into play. This, as per the recent ATLAS announcement [53] is constrained to be below 14%. In terms of signatures of inert doublet, we can have either pure leptonic final states plus missing transverse energy (MET) [54, 55], hadronic final states plus MET [56] or a mixture of both. In our model, MET may correspond to either neutrinos or singlet fermion DM. In another work [57], tri-lepton plus MET final states were also discussed, whereas mono-jet signatures have been studied by the authors of [58, 59]. Thus, the model offers interesting collider prospects as well while also getting constrained from existing data. The details of such collider prospects is beyond the scope of this present work and can be found elsewhere. Another important observable from the collider search is the Higgs to diphoton decay rate. The presence of the charged scalar, ϕ^+ , in the inert doublet will contribute to the $h \rightarrow \gamma\gamma$ through one loop process. The present CMS results [60] constrains the quantity $\frac{\text{BR}(h \rightarrow \gamma\gamma)_{\text{expt}}}{\text{BR}(h \rightarrow \gamma\gamma)_{\text{SM}}} = 1.12 \pm 0.09$ which implies the new contribution should be in the limit,

$$\frac{\text{BR}(h \rightarrow \gamma\gamma)_{\text{New}}}{\text{BR}(h \rightarrow \gamma\gamma)_{\text{expt}}} = 0.03 \text{ to } 0.17. \quad (20)$$

The additional contribution to the Higgs to diphoton branching ratio in our model arises from the charged component of the new scalar doublet (ϕ^\pm) and the corresponding Higgs coupling (λ_4). Throughout our analysis, we keep the mass of ϕ^\pm within the allowed range and the Higgs portal coupling, $\lambda_4 \sim \mathcal{O}(10^{-4})$, which keeps our model safe from the mentioned bound on Eq. (20).

III. NUMERICAL ANALYSIS

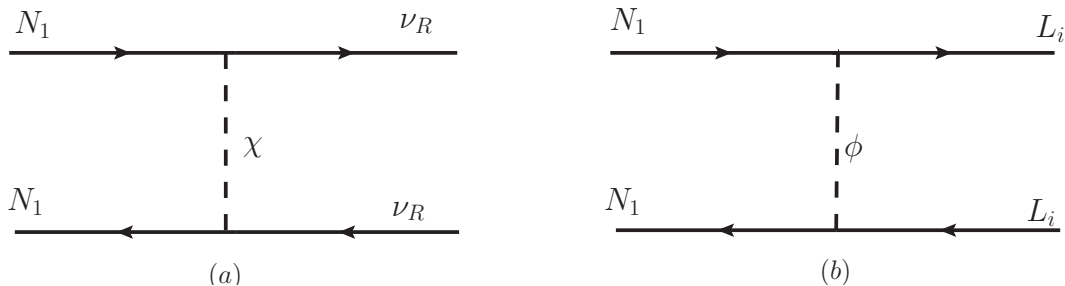


FIG. 2: Dominant DM annihilation processes. In the right panel Feynman diagram, ϕ corresponds to all the states of ϕ including ϕ^0, ϕ^\pm depending upon the final state lepton.

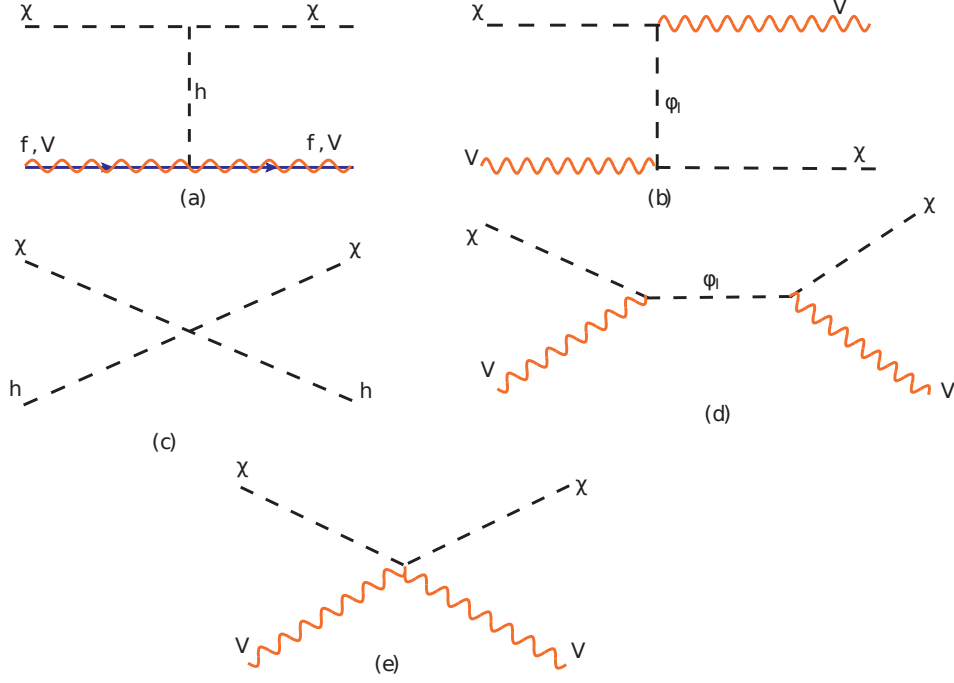


FIG. 3: Scattering processes associated with thermalisation of χ with the SM bath.

As mentioned earlier, we consider N_1 , the lightest Z_2 -odd particle to be the dark matter candidate. Being a gauge singlet fermion, its thermalisation and relic abundance will crucially depend upon the Yukawa interactions shown in Eq. (2). The dominant annihilation channels are shown in Fig. 2. However, the same Yukawa interactions are also constrained from neutrino mass criteria. However, neutrino mass also depends upon another free dimensionless parameter namely, the scalar mixing angle θ . Therefore, depending upon the mixing angle and Yukawa couplings, we have categorised our study into three separate scenarios as follows.

- Case-I: In this case, the Yukawa coupling associated with the singlet scalar (y_χ) is always greater than the one associated with the doublet scalar (y_ϕ) and the mixing angle is tiny ($\sin \theta \leq 10^{-4}$).
- Case-II: In this case also the Yukawa coupling associated with the singlet scalar (y_χ) is always greater than the Yukawa associated with the doublet scalar (y_ϕ); however, the mixing angle is large ($\sin \theta \sim 0.7$).
- Case-III: In this case, both the Yukawa couplings are taken to be in the same order and the mixing angle is fixed from neutrino mass bound.

If the mixing angle between χ and ϕ_R is tiny ($\sin \theta \leq 10^{-4}$)¹, then the process of kinetic decoupling of χ with the SM will be influenced by processes shown by the first four diagrams of Fig. 3. However, in a situation, where this mixing angle is large ($\sin \theta \sim 0.7$), the gauge boson scattering processes with χ will be the dominant channels for the kinetic decoupling process, shown by the last diagram of Fig. 3. The DM parameter space will not be affected in both cases since the relevant Yukawa couplings involved in DM thermalisation processes have already been fixed. On the contrary, ΔN_{eff} will be affected as it is heavily dependent upon the kinetic decoupling profile of χ , which acts like a portal between ν_R and the SM bath.

We follow the step-by-step procedure described below to establish a connection between dark matter and effective degrees of freedom, N_{eff} . We consider the masses for the singlet fermion and scalar as $M_{N_1} < M_\chi$ so that the decay $N_1 \rightarrow \chi + \nu_R$ is kinematically forbidden. To check the viability of the lightest fermion singlet N_1 as a dark matter candidate, we need to check the relic abundance at the present epoch. In the first two cases, since the Yukawa coupling associated with the singlet scalar (y_χ) is greater than the one with doublet scalar (y_ϕ), the DM sector gets decoupled from the SM sector at early epochs. After the singlet scalar χ gets kinetically decoupled from the SM bath along with the fermion singlet and ν_R , they do not maintain equilibrium temperature with the photons ($T_\gamma \neq T_{\nu_R}$). Here, we have used the notation T_{ν_R} as the temperature of the relativistic species for the dark sector temperature and T_γ as the SM bath temperature.

We first find the decoupling² temperature (T_{Dec}) of χ for its elastic scattering processes by the simple assumption $\frac{\Gamma}{H}|_{T_{\text{Dec}}} = 1$, where $\Gamma = \frac{\Gamma_{\text{el}}}{n_{\text{scat}}}$. Here, elastic scattering rate is $\Gamma_{\text{el}} = \sum_a n_a^{\text{eq}} \langle \sigma v \rangle_{\chi a \rightarrow a \chi}$ for the process $\chi a \rightarrow a \chi$, H is the Hubble expansion rate and a represents SM particles (both fermions and bosons). For a massive dark matter candidate χ of mass M_χ , the momentum transfer per collision with the plasma for $T \ll M_\chi$ is of the order T . This transferred momentum is much smaller than the average momentum of the DM candidate ($p \sim (M_\chi T)^{1/2}$). Therefore a number of collisions $n_{\text{scat}} \sim M_\chi T$, are required

¹ When the mixing is large (case-II), we can see from Eq.(8) that the physical eigenstates (or the mass eigenstates) and the interaction states are different; however, if the mixing is tiny (case-I and case-III), then mass eigenstates are similar to flavour eigenstates. Therefore, we use the terminology S_1, S_2 for case-II only and for the other two cases, we use χ and ϕ explicitly.

² As chemical decoupling has already occurred at a higher temperature, the final temperature of χ will be decided by its kinetic decoupling from the thermal bath.

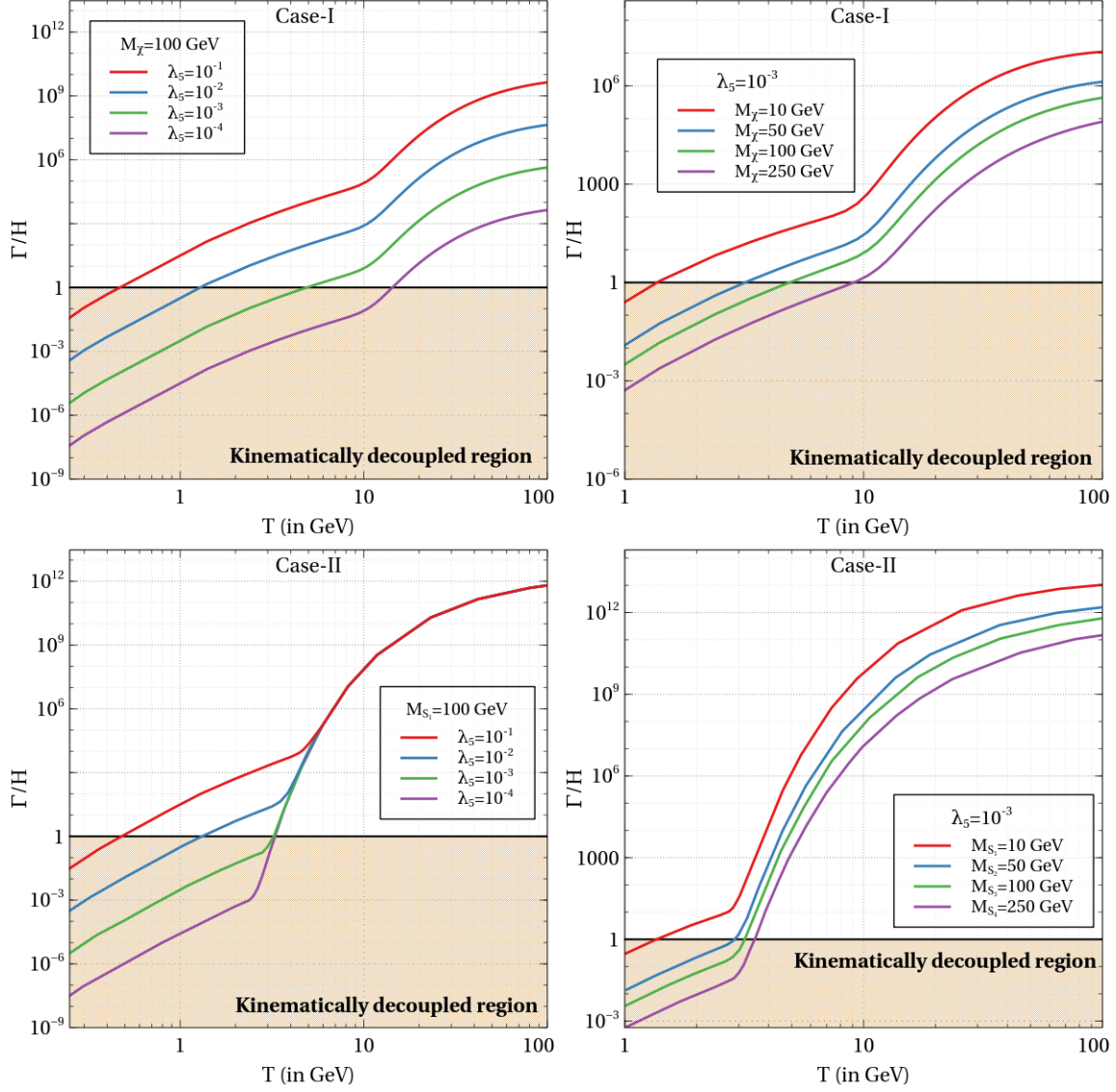


FIG. 4: Comparison of Γ/H for different choices of mass and quartic coupling λ_5 are shown for both case-I and case-II.

for the dark matter to transfer a large part of its momentum to the plasma or to acquire it from the plasma itself [61]. However, in case-III, we adopt the trivial method to find the relic abundance [62] as in this case, the DM sector evolves together with the SM plasma due to a similar choice of Yukawa couplings ($y_\phi \sim y_\chi$) and hence they share the same bath temperature. We find the kinetic decoupling temperature for both the DM as well as ν_R from their respective scattering processes. Whichever a particle decouples earlier, from that decoupling temperature itself ν_R temperature will start deviating from the SM bath, simply because ν_R can interact with the SM only via dark sector particles.

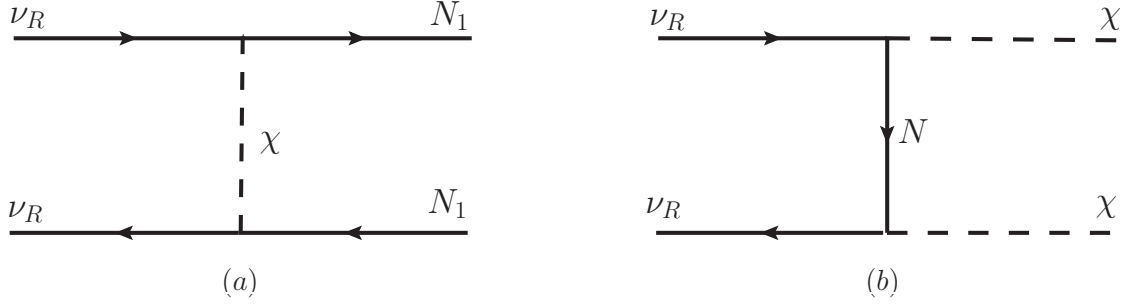


FIG. 5: Thermalisation of ν_R with the dark sector.

The kinetic decoupling profiles of the first two cases are shown in Fig. 4. In the left panel plots, we keep the singlet scalar mass fixed at 100 GeV and vary the Higgs portal quartic coupling within the range $\lambda_5 \in (10^{-1} - 10^{-4})$. We have fixed the quartic coupling in the right panel plots and chosen four benchmark values for χ masses. A clear difference is visible between case-I and case-II from the left panel plots. In the lower-left panel plot, the temperature evolution patterns for the normalised scattering rate overlap at a higher temperature showing a lack of dependence on quartic coupling. This is because of the dominance of the gauge coupling over others. For small mixing angle θ in case-I, such gauge portal interactions remain ineffective, leading to changes in scattering rate for different quartic couplings even at higher temperatures, as seen from the upper left panel plot of Fig. 4. The mixing depends on the Higgs VEV according to Eq. (8) and before the electroweak symmetry breaking (EWSB), there will not be any mixing. We are interested in the situation where the dark sector decouples from the visible sector at a low temperature ($T \sim 10$ GeV) as it will lead to a significant change in the ΔN_{eff} . For fixed quartic coupling but the change in mass, case-II gives rise to a narrower window of decoupling temperature as compared to case-I. In case-I, for λ_5 ranging from 10^{-1} to 10^{-4} , we can see decoupling temperatures shifting from 500 MeV to 10.2 GeV (top left panel plot of Fig. 4). On the other hand, for the singlet scalar mass ranging from 10 GeV to 250 GeV, we can see a shift in decoupling temperature from 1.2 GeV to around 10 GeV (top right panel plot of Fig. 4). However, in the lower panels for case-II, we can see shrinking decoupling regions for the same benchmark points due to unsuppressed gauge interactions. The contribution to ΔN_{eff} strictly depends on the kinetic decoupling temperature of ν_R . From the decoupling profile study in case-II, we see a narrow separation among the decoupling temperatures as

compared to case-I. This would lead to a minor relative change in ΔN_{eff} calculations, hence we skip the ΔN_{eff} calculation for case-II and focus completely on case-I and case-III. The thermalisation processes for ν_R are shown in Fig. 5.

Case-I ($y_\chi \gg y_\phi$): In this case, for the evolution of the dark sector as well as ν_R , we have two distinct regions separated by the decoupling temperature T_{Dec} : *Region I* ($T \geq T_{\text{Dec}}$) and *Region II* ($T \leq T_{\text{Dec}}$). In region-I, all the species (SM+dark sector) are maintaining kinetic equilibrium with each other and sharing a common temperature T_γ . Therefore, we can define a reduced Boltzmann equation for the two species χ and N_1 (DM) into a single one with total comoving number density $Y(= \frac{n}{s}) = Y_\chi + Y_{\text{DM}}$ as,

$$\frac{dY}{dx} = -\frac{1}{2} \frac{\beta s}{\mathbf{H}x} \langle \sigma v \rangle_{\text{eff}} [Y^2 - Y_{\text{eq}}^2]. \quad (21)$$

Here, with an arbitrary mass scale M_0 we have defined $x = M_0/T$, $s(T) = g_*(T) \frac{2\pi^2 T^3}{45}$ being the entropy density, $\mathbf{H}(T) = \sqrt{\frac{8g_*(T)}{\pi}} \frac{T^2}{M_{\text{Pl}}}$ is the Hubble rate with $g_*(T)$ as the effective relativistic degrees of freedom at temperature T . We have also defined a parameter $\beta(T) = \frac{g_*^{1/2}(T) \sqrt{g_\rho(T)}}{g_s(T)}$ with g_s and g_ρ being the effective relativistic degrees of freedom for entropy and energy densities respectively. Here, $g_*^{1/2}$ is defined as $g_*^{1/2} = \frac{g_s}{\sqrt{g_\rho}} \left(1 + \frac{1}{3} \frac{T}{g_s} \frac{dg_s}{dT}\right)$. The effective annihilation cross-section for the combined processes is given by [63]

$$\langle \sigma v \rangle_{\text{eff}} = \frac{\langle \sigma v \rangle_{\text{DMD}\bar{\text{M}} \rightarrow \nu_R \bar{\nu}_R} (Y_{\text{DM}}^{\text{eq}})^2 + \langle \sigma v \rangle_{\chi\chi \rightarrow X\bar{X}, \nu_R \bar{\nu}_R} (Y_\chi^{\text{eq}})^2}{(Y_{\text{DM}}^{\text{eq}} + Y_\chi^{\text{eq}})^2}. \quad (22)$$

Here, $\chi\chi \rightarrow X\bar{X}$ represents the pair annihilation of χ into the SM species through the Higgs portal interactions.

Now, for region-II, the dark sector has decoupled from the SM bath and maintains a local thermodynamic equilibrium among χ , N_1 and ν_R due to strong Yukawa interaction (y_χ) with a common temperature $T_{\nu_R} \neq T_\gamma$. We have chosen the Yukawa y_ϕ to be tiny ($\sim \mathcal{O}(10^{-6})$). Such choices of parameters do satisfy the light neutrino mass and at the same time, also allow N_i to evolve with the dark sector; finally, such small Yukawa coupling with the charged lepton keeps our model safe from the lepton flavour violation constraints. In this region-II, since SM and dark sector temperatures are different, we defined a quantity $\xi = \frac{T_{\nu_R}}{T_\gamma}$ to keep track of the difference in temperatures of the two sectors effectively. Therefore, we can now redefine the coupled Boltzmann equations as follows [23]

$$\frac{dY}{dx} = -\frac{1}{2} \frac{\beta s}{\mathbf{H}x} \langle \sigma v \rangle_{\text{eff}} [Y^2 - Y_{\text{eq}}^2], \quad (23)$$

$$x \frac{d\xi}{dx} + (\beta - 1)\xi = \frac{1}{2} \frac{\beta x^4 s^2}{4\alpha \xi^3 \mathbf{H} M_0^4} \langle E \sigma v \rangle_{\text{eff}} [Y^2 - Y_{\text{eq}}^2]. \quad (24)$$

Here, $\alpha = g_i \frac{7}{8} \frac{\pi^2}{30}$ with g_i being the relativistic degree of freedom. We have defined the effective thermal averaged cross-section as

$$\langle E\sigma v \rangle_{\text{eff}} = \frac{\langle E\sigma v \rangle'_{\nu_R \bar{\nu}_R \rightarrow \text{DMDM}} (Y_{\text{DM}}^{\text{eq}})^2 + \langle E\sigma v \rangle'_{\nu_R \bar{\nu}_R \rightarrow \chi\chi} (Y_{\chi}^{\text{eq}})^2}{(Y_{\text{DM}}^{\text{eq}} + Y_{\chi}^{\text{eq}})^2}, \quad (25)$$

where, $\langle E\sigma v \rangle'_{x\bar{x} \rightarrow y\bar{y}}$ is the thermal average of $E \times \sigma v_{x\bar{x} \rightarrow y\bar{y}}$ normalized by the product of equilibrium number densities of the final state particles *i.e.*, $n_y^{\text{eq}} n_{\bar{y}}^{\text{eq}}$. The primary difference between the evolution of comoving number densities in region-I and region-II is that the former only depends on a single temperature (T_γ) while the latter's evolution is a function of both the temperatures (T_γ & T_{ν_R}). In the appendix of Ref. [23], one can find a detailed derivation of the Boltzmann equation for ξ along with related terms, and cross-sections associated with it.

We show the impact of Higgs portal couplings and χ mass on the temperature ratio (T_{ν_R}/T_γ) in Fig. 6. For the tiny scalar mixing (case-I) we can see a sizable contribution for temperature ratio, which will lead to a sizable contribution to N_{eff} . However, for the large scalar mixing parameter (case-II), the contributions are relatively weaker for the same choice of other model parameters. Therefore, further analysis of the effective relativistic degree of freedom in case-II would be less significant compared to case-I in this model.

In case-III, due to equal strength in Yukawa couplings, both dark sector and SM evolution occur together. After dark sector freeze-out, both DM and ν_R decouple at a particular temperature. We find the kinetic decoupling temperatures for both species by comparing their scattering rates with the Hubble expansion rate as defined earlier for case-I. The comparison is shown in the left panel plot of Fig. 7 while the right panel plot shows the corresponding decoupling temperatures for two benchmark points. Clearly, the DM scattering processes decouple prior to the ν_R scattering processes.

Since we are considering a Dirac neutrino framework, the right chiral counterparts ν_R are as light as the corresponding left chiral neutrinos, hence we get an additional contribution to N_{eff} , leading to a non-zero $\Delta N_{\text{eff}} (= N_{\text{eff}} - N_{\text{eff}}^{\text{SM}})$. For the N_{eff} calculation, we have considered the instantaneous decoupling of three ν_R 's and also ignored the role of lepton flavour effects. While instantaneous decoupling never happens in reality, but it can be taken as a good approximation [17]. As soon as the singlet scalar χ decouples from the SM plasma, it drags the dark sector along with it due to strong Yukawa interaction (y_χ). We have also assumed that all the three ν_R 's do have similar Yukawa coupling such that we can consider equally

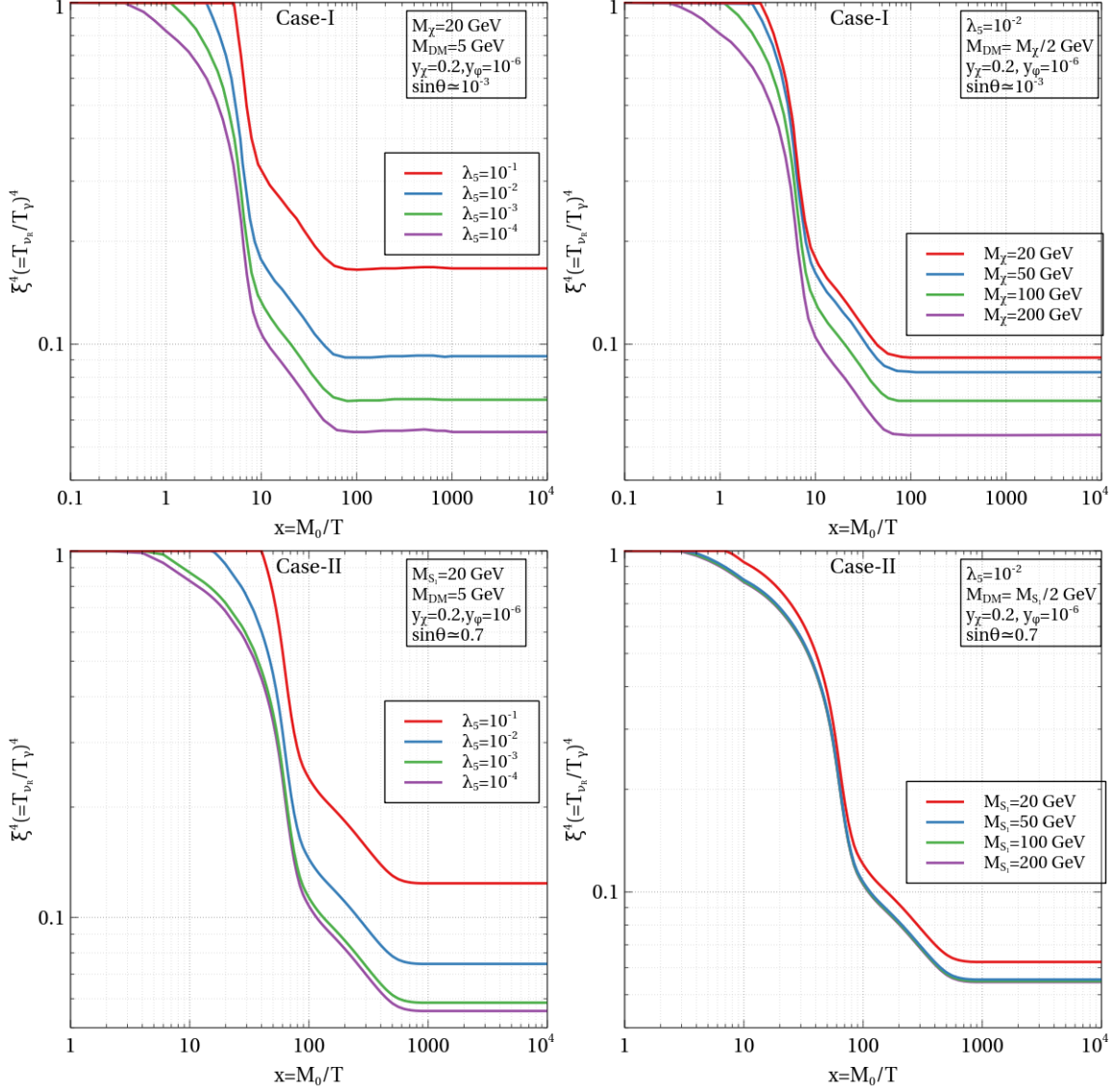


FIG. 6: Variation of the temperature ratio $(\frac{T_{\nu_R}}{T_\gamma})^4$ with x for different Higgs portal coupling and masses.

distributed energy density for all the three species *i.e.*, $\sum_i \rho_{\nu_{Ri}} = 3 \times \rho_{\nu_{Ri}}$. The effective number of degrees of freedom is defined as the ratio between the radiation energy density of the non-photon contribution to the radiation energy density of a single SM neutrino species

$$N_{\text{eff}} = \frac{\rho_{\text{rad}} - \rho_\gamma}{\rho_{\nu_L}}, \quad (26)$$

where ρ_{ν_L} is the energy density of one active neutrino. Hence from this definition, we can

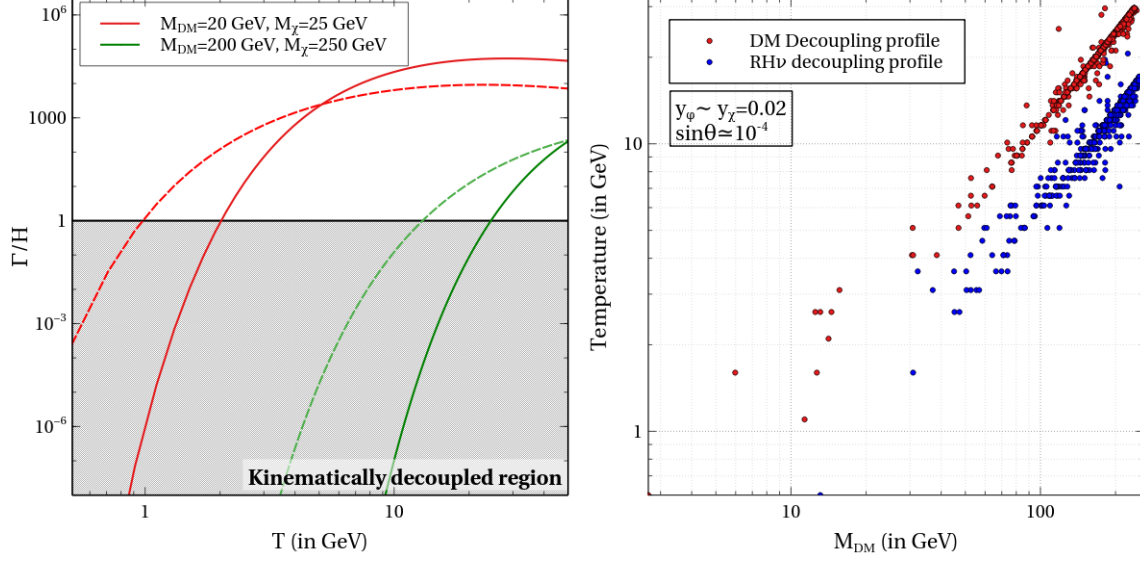


FIG. 7: *Left panel:* The solid and dashed lines represent dark matter and ν_R decoupling patterns for two benchmark points indicated by two colours. *Right panel:* Decoupling temperatures of DM and right-handed neutrinos for the complete mass range.

finally define the ΔN_{eff} for three generations of neutrinos as³:

$$\Delta N_{\text{eff}} = \frac{\sum_\alpha \rho_{\nu_R^\alpha}}{\rho_{\nu_L}} = 3 \left(\frac{\rho_{\nu_R}}{\rho_{\nu_L}} \right) \Big|_{T > T_{\nu_L}^{\text{dec}}} = 3 \times \left(\frac{T_{\nu_R}}{T_\gamma} \right)^4 \Big|_{T > T_{\nu_L}^{\text{dec}}} = 3 \times \xi^4. \quad (27)$$

Here, we have used the bath temperature (T_γ) instead of the temperature of active neutrinos T_{ν_L} . This is because, above the decoupling temperature of ν_L ($T_{\nu_L}^{\text{dec}}$), both active neutrinos and photons share the same temperature. Consequently, it is not essential to track the temperature of ν_R till recombination as the ratio of T_{ν_R} and T_{ν_L} remains constant just after active neutrinos decouple from the thermal bath. Therefore, we have restricted our numerical analysis till $T_{\nu_L}^{\text{dec}}$.

IV. RESULTS AND DISCUSSION

For numerical analysis, we considered broad parameter regions for both dark matter and N_{eff} calculations, as shown in table II for all the cases mentioned above. As noted earlier, one of the neutral components of inert doublet can still be as light as a few GeV provided the other component masses are chosen appropriately to satisfy the LEP limits. Throughout

³ For massless species $\rho \propto T^4$.

Cases	Parameters	Chosen range
All	Dark matter mass	$M_{\text{DM}} = [1, 250] \text{ GeV}$
	Singlet scalar mass	$M_\chi = [1, 350] \text{ GeV}$
	Doublet masses (For ϕ^\pm, ϕ^0)	$M_\phi = [1, 350] \text{ GeV}$
	Mass separation ($M_i - M_{\text{DM}}$)	$\Delta M = [1, 100] \text{ GeV}$
	Higgs portal coupling	$\lambda_5 = [10^{-4}, 10^{-1}]$
Case-I &Case-II	Yukawa coupling with χ	$y_\chi = 0.2 \text{ (fixed)}$
	Yukawa coupling with ϕ	$y_\phi \simeq 10^{-6} \text{ (fixed)}$
	Mixing angle (Case-I)	$\sin \theta \sim 10^{-6}$
	Mixing angle (Case-II)	$\sin \theta \sim 10^{-2}$
Case-III	1. Yukawa coupling with χ & ϕ	$y_\chi \sim y_\phi = 0.2 \text{ (fixed)}$
	Mixing angle	$\sin \theta \sim 10^{-5}$
	2. Yukawa coupling with χ & ϕ	$y_\chi \sim y_\phi = 0.02 \text{ (fixed)}$
	Mixing angle	$\sin \theta \sim 10^{-4}$

TABLE II: The choice of parameter ranges for all three cases in our study.

our numerical analysis, the choices of Yukawa couplings are fixed in such a manner that they do satisfy neutrino mass bounds. We now present our results for these cases one by one.

1. Case-I:

For the dark matter relic calculation, we developed our own code and solved the relevant Boltzmann equations numerically to get relic abundance. As discussed earlier, the dark sector decouples from the SM sector once the kinetic equilibrium between the two sectors is lost. Therefore, we first solved the Boltzmann Eq. (21) till the decoupling temperature T_{Dec} to find the initial abundance for the dark sector particles. Then we solve the coupled BEs (Eq. (24)) from the T_{Dec} to a very low temperature to find the relic abundance of DM. Among the annihilation processes of DM, the charged scalar mediated $\text{DM} \overline{\text{DM}} \rightarrow l_\alpha \bar{l}_\beta$ processes remain sub-dominant due to the choice of tiny Yukawa couplings associated with charged leptons.

Fig. 8 shows the allowed parameter space of dark matter mass with Higgs portal couplings

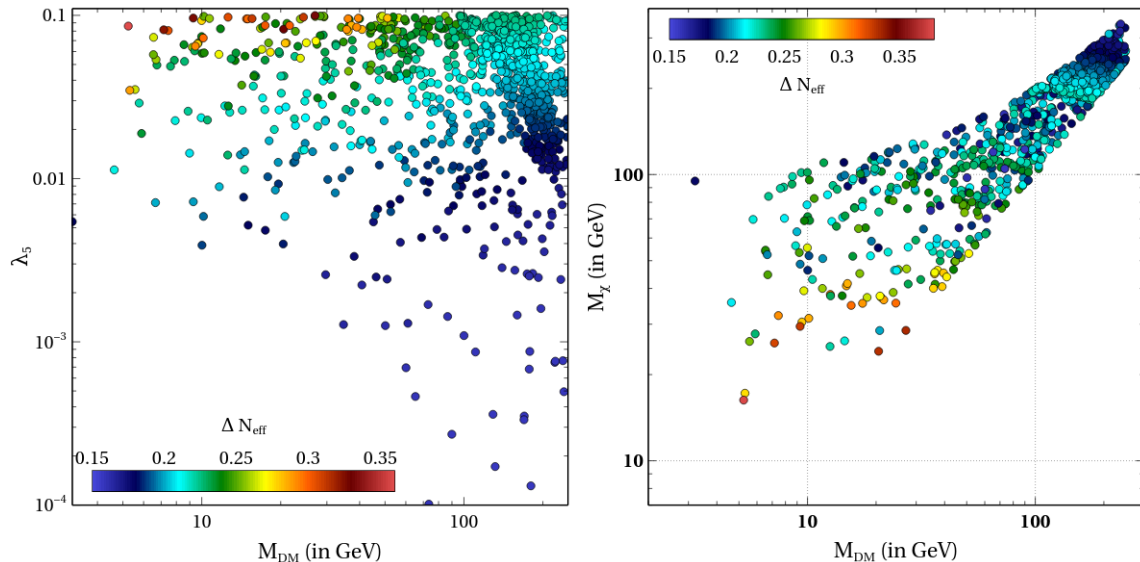


FIG. 8: Allowed parameter space satisfying the correct relic density (within 3σ C.L.) of DM and all other experimental constraints such as neutrino mass, LEP and collider is shown in $M_{DM} - \lambda_5$ plane (Left panel) and in $M_{DM} - M_\chi$ plane (Right panel) where the color band represents the dependence on ΔN_{eff} .

(λ_5) and the singlet scalar mass (M_χ) while choosing other parameters as shown in table II. We have adopted the logarithmic approach to generate random points while carrying out our numerical analysis. All the points in the plane satisfy the current 3σ bound of dark matter relic abundance ($0.117 > \Omega h^2 > 0.123$). In the M_{DM} versus M_χ plot shown on the right panel, there is a clear preference for high mass DM with singlet scalar mass being close to M_{DM} for efficient coannihilations. From Eq. (9), it is clear that both the masses, M_{DM} and M_χ are related to neutrino mass.

In Fig. 9, we show the dependence of ΔN_{eff} with quartic coupling (λ_5) with the colour bars in left and right panels showing the variation in singlet scalar and DM masses respectively. One can see the gradual increase in ΔN_{eff} values with an increase in λ_5 and a decrease in masses. This is expected as larger coupling or smaller masses lead to late decoupling of ν_R from the bath. The shaded region above the blue dashed horizontal line is the excluded region from the Planck 2018 constraint at 2σ C.L. ($\Delta N_{\text{eff}} \leq 0.285$ [2]). The other three dashed horizontal lines are respectively the bounds from Planck-2018 at 1σ C.L. ($\Delta N_{\text{eff}} = 0.12$ [2], red dashed line), SPT-3G at 1σ ($\Delta N_{\text{eff}} = 0.1$ [64], magenta dotted line) and CMB-S4 at 2σ ($\Delta N_{\text{eff}} = 0.06$ [65], black dot-dashed line). Clearly, the entire parameter space remains

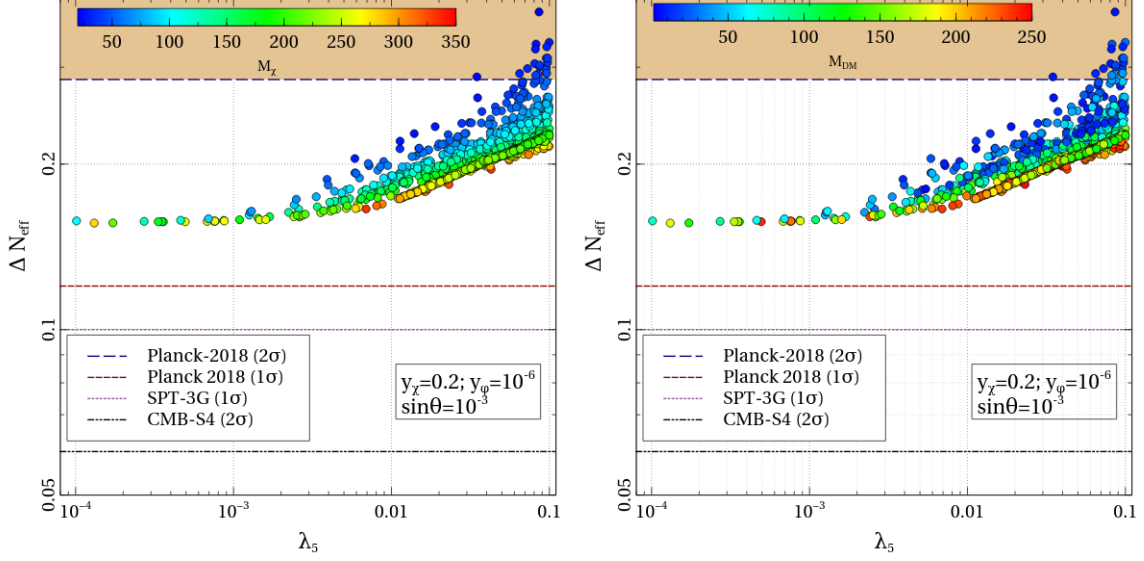


FIG. 9: Dependence of ΔN_{eff} with the Higgs- χ quartic coupling (λ_5) in case-I. The colour bar in the left (right) panel plot shows singlet scalar mass M_χ (dark matter mass M_{DM}). All the points do satisfy bounds related to DM, neutrino mass, LFV, LEP and colliders.

within future sensitivities.

2. Case-III

In this case, we have considered two sub-scenarios by choosing two different Yukawa couplings (while maintaining equality $y_\phi = y_\chi$) with corresponding scalar mixing angles to be consistent with neutrino mass bound. The choices of numerical values of different parameters are shown in table II. To carry out the numerical analysis, we first find the DM relic abundance using `micrOmegas` [66] and then find the decoupling profile for both the DM and ν_R for respective scattering processes. This case differs from the earlier two cases due to the choice of equal Yukawa couplings.

In Fig. 10, we show how ΔN_{eff} depends on dark matter mass for both the choice of Yukawa couplings. We show the decoupling temperatures in the colour band in each case. The horizontal lines correspond to the same bounds and sensitivities for ΔN_{eff} as mentioned while discussing Fig. 9 for case-I. For most of the points, one may notice that the contribution to ΔN_{eff} remains below the current Planck 2018 2σ bound while being within future sensitivities.

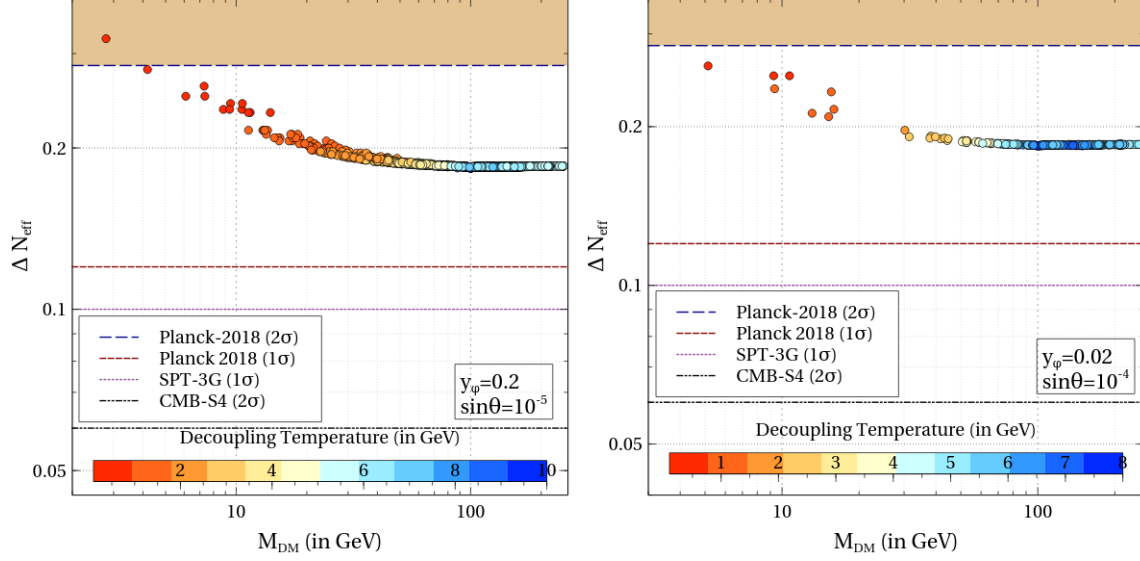


FIG. 10: Dependence of ΔN_{eff} with dark matter mass for case-III for two different choices of Yukawa couplings and scalar mixing angles. The colour band indicates the decoupling temperature of the dark matter candidate. All the points do satisfy bounds related to DM, neutrino mass, LEP and colliders.

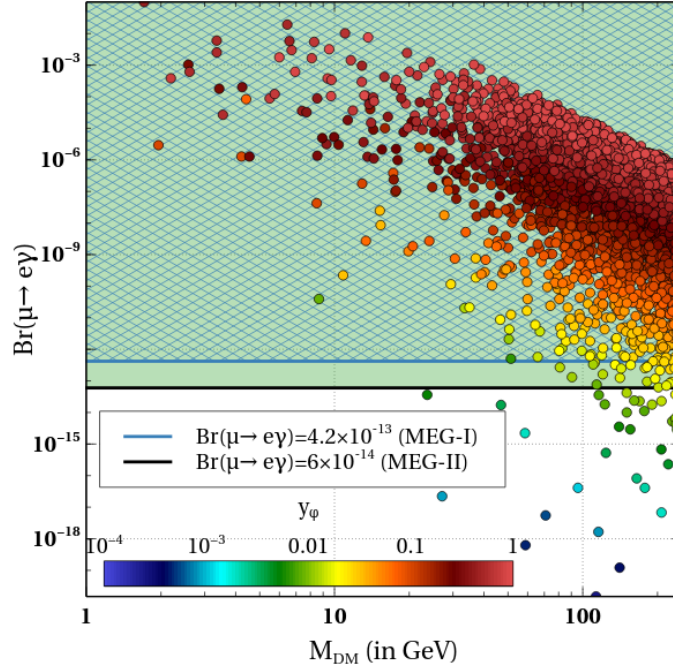


FIG. 11: $\text{Br}(\mu \rightarrow e\gamma)$ versus DM mass with varying Yukawa coupling (y_ϕ). We have shown the variation of Yukawa coupling (y_ϕ) in the colour bar. The shaded regions correspond to the currently excluded regions from MEG-I [43] and MEG-II [45] experiments, as shown in the key.

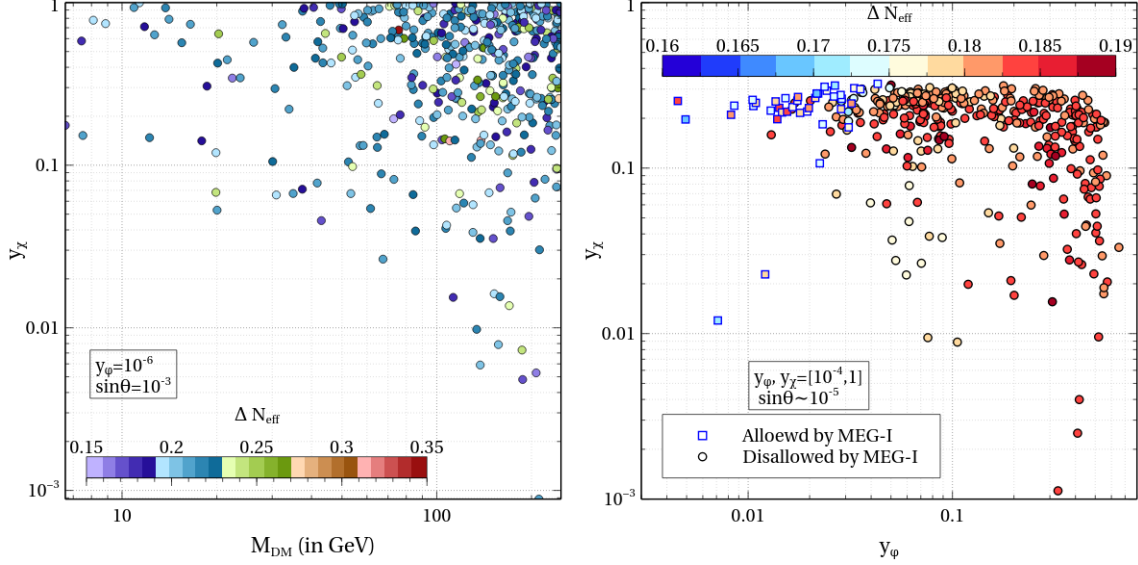


FIG. 12: *Left panel:* Allowed parameter space in the $y_\chi - M_{DM}$ (*left*) and $y_\chi - y_\phi$ plane satisfying the current 3σ bound on DM relic abundances, neutrino mass, LEP and collider constraints. The colour bar indicates the corresponding ΔN_{eff} values.

It should be noted that due to small Yukawa coupling $y_\phi = 10^{-6}$ in case-I, case-II, it is trivial to satisfy the LFV bounds. However, this need not be so in case-III with large Yukawa couplings. Therefore, we explicitly calculate $\text{Br}(\mu \rightarrow e\gamma)$ for the parameter choices in case-III and show its variation with dark matter mass for a range of Yukawa coupling in Fig. 11. While in Fig. 10, we considered two different choices of y_ϕ ($y_\phi = 0.2$ and $y_\phi = 0.02$) to show ΔN_{eff} results, from Fig. 11, we can now see that one of these choices namely, $y_\phi = 0.2$ is completely ruled out from current LFV bounds. Thus, a large part of the parameter space with sizeable Yukawa coupling y_ϕ is already disfavoured from LFV searches, with a considerable amount of parameter space being within reach of future LFV searches. While a future discovery of LFV decay $\mu \rightarrow e\gamma$ will definitely indicate an observable ΔN_{eff} at future CMB experiments within the purview of this model, but not vice versa. This nevertheless keeps the complementary detection prospects of the model very promising.

Finally, instead of choosing specific Yukawa couplings as in case-I and case-III discussed above, we perform a numerical scan over them. In the left panel of Fig. 12, we show the allowed points of Yukawa coupling y_χ with dark matter mass, while the other Yukawa coupling y_ϕ is kept fixed at 10^{-6} . In the right panel plot of Fig. 12, we show the mutual allowed points in a plane with both of these Yukawa couplings in respective axes. All the

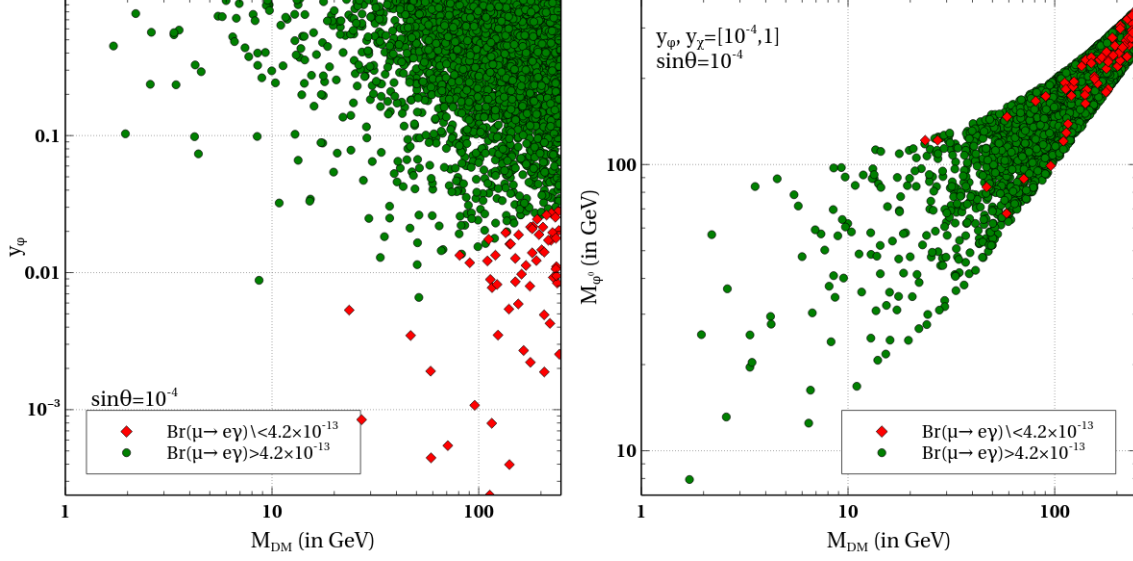


FIG. 13: Allowed parameter space in the y_ϕ vs. M_{DM} (left) and M_{DM} vs. M_{ϕ^0} (right) plane satisfy the current 3σ relic abundance bound for dark matter and relevant experimental constraints.

points in Fig. (12) satisfy the current 3σ bound on DM relic abundances, neutrino mass and collider bounds. The colour bar in both plots indicates the corresponding ΔN_{eff} value. Clearly, some of the points are already ruled out by Planck 2018 2σ bound on ΔN_{eff} and MEG-I bound on $\mu \rightarrow e\gamma$. In Fig. 13, we show the final allowed parameter space allowed from all constraints except the LFV bounds. The red square-shaped (green circular) points indicate the ones allowed (disallowed) by MEG-I constraints on LFV decay $\mu \rightarrow e\gamma$. In the left panel, we have shown the allowed region in the y_ϕ vs. dark matter mass M_{DM} plane, while on the right panel, we display the allowed region in $M_{\phi^0} - M_{DM}$ plane. Clearly, a large part of the parameter space already saturates the current LFV bounds.

Finally, we show the direct detection prospects of DM in our setup. Clearly, DM does not have any tree-level scattering process off nucleons. However, at the one-loop level, we can have a direct detection cross-section as shown in Fig. 14. The contribution to the spin-independent scattering cross-section for the dark matter-nucleon scattering is given by

$$\sigma_{\text{SI}} = \left(\frac{m_n}{v}\right)^2 \frac{\mu_{\text{DMn}}^2 g_{NNh}^2}{\pi M_h^4} f_n^2 \quad (28)$$

where $f_n = 0.3$ depends on the quark content within a nucleon for each quark flavour[67], $\mu_{\text{DMn}} = \frac{M_{\text{DM}} m_n}{M_{\text{DM}} + m_n}$ is the reduced mass of DM-nucleon system with m_n being the mass of the

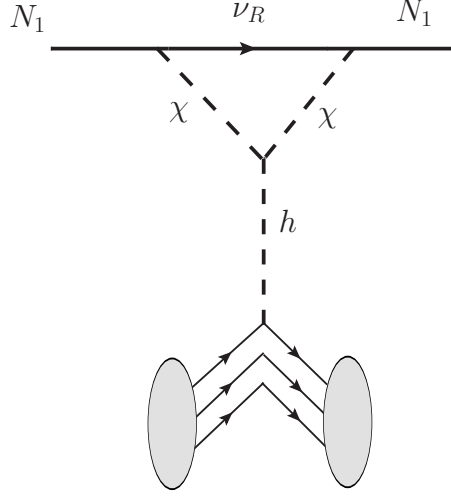


FIG. 14: Schematic diagram for one-loop dark matter scattering off nucleon via SM Higgs

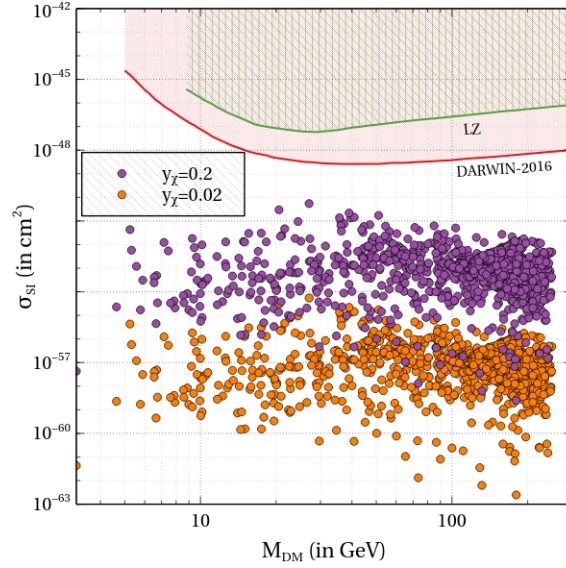


FIG. 15: Spin-independent scattering cross-section of DM for two different choices of Yukawa couplings y_χ .

nucleon. The effective coupling between DM and Higgs can be written as

$$g_{\bar{N}N h} = \frac{i}{16\pi^2} \times \frac{y_\chi \lambda_5 v}{M_{\text{DM}}} \times \left[1 + \left(\frac{M_\chi^2}{M_{\text{DM}}^2} - 1 \right) \ln \left(1 - \frac{M_{\text{DM}}^2}{M_\phi^2} \right) \right]. \quad (29)$$

As only the singlet scalar χ is involved in the direct detection processes, we check the spin-independent cross-section with two choices of Yukawa couplings y_χ . The other relevant parameters are kept in the same range specified in table II. From Fig. 15, we can see that all

the points in the σ_{SI} *vs.* M_{DM} plane is well below the recent bounds from LZ experiment [4] shown by green curve, future sensitivity of DARWIN experiment [68] shown by red curve⁴.

V. CONCLUSION

We have studied the possibility of probing the Dirac scotogenic model via future CMB observations by considering fermion singlet DM. Since fermion singlet DM annihilates primarily via Yukawa interactions, the same interactions can also lead to the thermalisation of Dirac neutrinos leading to enhanced ΔN_{eff} . We consider all possible choices of DM Yukawa couplings as well as scalar mixing angle in our analysis. The Planck upper bound on the sum of the neutrino masses as well as the overall neutrino mass constraint, allows us to choose the Yukawa couplings and the mixing angle in such a way that gives rise to three distinct parameter regimes in this model. In each of these cases, we discuss and show the detection prospects of the model while being consistent with the desired DM phenomenology and neutrino mass constraints. While some part of the parameter space is already ruled out by the Planck 2018 upper bound on ΔN_{eff} , the currently allowed parameter space remains within the future sensitivity of experiments like CMB-S4. While direct detection prospects remain low for such fermion singlet DM due to radiative suppression of DM-nucleon scattering cross-section, some part of the parameter space is already ruled out by constraints from charged lepton flavour violation and collider bounds. It is worth mentioning that the detection of LFV decay $\mu \rightarrow e\gamma$ in the future would imply an observable ΔN_{eff} in forthcoming CMB experiments within the framework of this Dirac scotogenic model. However, the reverse relationship is not necessarily true. These complementary detection prospects of such DM scenarios with suppressed direct detection rates are particularly interesting in view of the relentless negative searches of WIMP DM at direct detection experiments so far.

VI. ACKNOWLEDGEMENTS

The work of DN is supported by National Research Foundation of Korea (NRF)’s grants with grant no. 2019R1A2C3005009(DN). PD would like to acknowledge IITG for the fi-

⁴ In [23], a relatively larger value of spin-independent cross-section for the same one-loop diagram was obtained due to a missing factor in the numerical calculation.

nancial support under the project grant number: IITG/R&D/IPDF/2021-22/20210911916. PD also thanks Nayan Das for the useful discussions at the early stage of this work. The work of DB is supported by Science and Engineering Research Board (SERB), Government of India grant MTR/2022/000575.

-
- [1] PARTICLE DATA GROUP collaboration, Review of Particle Physics, [PTEP](#) **2020** (2020) [083C01](#).
 - [2] PLANCK collaboration, Planck 2018 results. VI. Cosmological parameters, [Astron. Astrophys.](#) **641** (2020) [A6](#) [[1807.06209](#)].
 - [3] G. Arcadi, M. Dutra, P. Ghosh, M. Lindner, Y. Mambrini, M. Pierre et al., The Waning of the WIMP? A Review of Models, Searches, and Constraints, [1703.07364](#).
 - [4] LUX-ZEPLIN collaboration, First Dark Matter Search Results from the LUX-ZEPLIN (LZ) Experiment, [2207.03764](#).
 - [5] E. Ma, Verifiable radiative seesaw mechanism of neutrino mass and dark matter, [Phys. Rev. D](#) **73** (2006) 077301 [[hep-ph/0601225](#)].
 - [6] R. H. Cyburt, B. D. Fields, K. A. Olive and T.-H. Yeh, Big Bang Nucleosynthesis: 2015, [Rev. Mod. Phys.](#) **88** (2016) 015004 [[1505.01076](#)].
 - [7] G. Mangano, G. Miele, S. Pastor, T. Pinto, O. Pisanti and P. D. Serpico, Relic neutrino decoupling including flavor oscillations, [Nucl. Phys. B](#) **729** (2005) 221 [[hep-ph/0506164](#)].
 - [8] E. Grohs, G. M. Fuller, C. T. Kishimoto, M. W. Paris and A. Vlasenko, Neutrino energy transport in weak decoupling and big bang nucleosynthesis, [Phys. Rev. D](#) **93** (2016) 083522 [[1512.02205](#)].
 - [9] P. F. de Salas and S. Pastor, Relic neutrino decoupling with flavour oscillations revisited, [JCAP](#) **1607** (2016) 051 [[1606.06986](#)].
 - [10] J. Froustey, C. Pitrou and M. C. Volpe, Neutrino decoupling including flavour oscillations and primordial nucleosynthesis, [JCAP](#) **12** (2020) 015 [[2008.01074](#)].
 - [11] J. J. Bennett, G. Buldgen, P. F. De Salas, M. Drewes, S. Gariazzo, S. Pastor et al., Towards a precision calculation of N_{eff} in the Standard Model II: Neutrino decoupling in the presence of flavo

- [JCAP 04 \(2021\) 073](#) [[2012.02726](#)].
- [12] K. Abazajian et al., CMB-S4 Science Case, Reference Design, and Project Plan, [1907.04473](#).
- [13] K. N. Abazajian and J. Heeck,
Observing Dirac neutrinos in the cosmic microwave background, [Phys. Rev. D100 \(2019\) 075027](#) [[1908.03286](#)].
- [14] P. Fileviez Pérez, C. Murgui and A. D. Plascencia,
Neutrino-Dark Matter Connections in Gauge Theories, [Phys. Rev. D100 \(2019\) 035041](#) [[1905.06344](#)].
- [15] D. Nanda and D. Borah,
Connecting Light Dirac Neutrinos to a Multi-component Dark Matter Scenario in Gauged $B - L$ Model, [1911.04703](#).
- [16] C. Han, M. López-Ibáñez, B. Peng and J. M. Yang,
Dirac dark matter in $U(1)_{B-L}$ with Stueckelberg mechanism, [2001.04078](#).
- [17] X. Luo, W. Rodejohann and X.-J. Xu, Dirac neutrinos and N_{eff} , [JCAP 06 \(2020\) 058](#) [[2005.01629](#)].
- [18] D. Borah, A. Dasgupta, C. Majumdar and D. Nanda,
Observing left-right symmetry in the cosmic microwave background, [Phys. Rev. D 102 \(2020\) 035025](#) [[2005.02343](#)].
- [19] P. Adshead, Y. Cui, A. J. Long and M. Shamma,
Unraveling the Dirac Neutrino with Cosmological and Terrestrial Detectors, [2009.07852](#).
- [20] X. Luo, W. Rodejohann and X.-J. Xu, Dirac neutrinos and N_{eff} II: the freeze-in case, [2011.13059](#).
- [21] D. Mahanta and D. Borah,
Low scale Dirac leptogenesis and dark matter with observable ΔN_{eff} , [2101.02092](#).
- [22] Y. Du and J.-H. Yu,
Neutrino non-standard interactions meet precision measurements of N_{eff} , [2101.10475](#).
- [23] A. Biswas, D. Borah and D. Nanda,
Light Dirac neutrino portal dark matter with observable ΔN_{eff} , [JCAP 10 \(2021\) 002](#) [[2103.05648](#)].
- [24] D. Borah, S. Mahapatra, D. Nanda and N. Sahu,
Type II Dirac Seesaw with Observable ΔN_{eff} in the light of W-mass Anomaly, [2204.08266](#).

- [25] S.-P. Li, X.-Q. Li, X.-S. Yan and Y.-D. Yang,
Effective neutrino number shift from keV-vacuum neutrinophilic 2HDM, [2202.10250](#).
- [26] A. Biswas, D. K. Ghosh and D. Nanda,
Concealing Dirac neutrinos from cosmic microwave background, [JCAP 10 \(2022\) 006](#)
[\[2206.13710\]](#).
- [27] A. Biswas, D. Borah, N. Das and D. Nanda,
Freeze-in Dark Matter and ΔN_{eff} via Light Dirac Neutrino Portal, [2205.01144](#).
- [28] Y. Cai, J. Herrero-García, M. A. Schmidt, A. Vicente and R. R. Volkas,
From the trees to the forest: a review of radiative neutrino mass models, [Front. in Phys. 5](#)
[\(2017\) 63](#) [[1706.08524](#)].
- [29] P.-H. Gu and U. Sarkar, Radiative Neutrino Mass, Dark Matter and Leptogenesis, [Phys. Rev. D 77 \(2008\) 105031](#) [[0712.2933](#)].
- [30] Y. Farzan and E. Ma, Dirac neutrino mass generation from dark matter, [Phys. Rev. D 86](#)
[\(2012\) 033007](#) [[1204.4890](#)].
- [31] D. Borah and A. Dasgupta,
Common Origin of Neutrino Mass, Dark Matter and Dirac Leptogenesis, [JCAP 12 \(2016\)](#)
[034](#) [[1608.03872](#)].
- [32] E. Ma and O. Popov, Pathways to Naturally Small Dirac Neutrino Masses, [Phys. Lett. B](#)
[764 \(2017\) 142](#) [[1609.02538](#)].
- [33] D. Borah and A. Dasgupta, Naturally Light Dirac Neutrino in Left-Right Symmetric Model,
[JCAP 06 \(2017\) 003](#) [[1702.02877](#)].
- [34] W. Wang, R. Wang, Z.-L. Han and J.-Z. Han,
The $B - L$ Scotogenic Models for Dirac Neutrino Masses, [Eur. Phys. J. C 77 \(2017\) 889](#)
[\[1705.00414\]](#).
- [35] E. Ma, Scotogenic cobimaximal Dirac neutrino mixing from $\Delta(27)$ and $U(1)_X$, [Eur. Phys. J. C 79 \(2019\) 903](#) [[1905.01535](#)].
- [36] E. Ma, Scotogenic $U(1)_X$ Dirac neutrinos, [Phys. Lett. B 793 \(2019\) 411](#) [[1901.09091](#)].
- [37] E. Ma, Leptonic Source of Dark Matter and Radiative Majorana or Dirac Neutrino Mass,
[Phys. Lett. B 809 \(2020\) 135736](#) [[1912.11950](#)].
- [38] J. Leite, A. Morales, J. W. F. Valle and C. A. Vaquera-Araujo,
Scotogenic dark matter and Dirac neutrinos from unbroken gauged $B - L$ symmetry, [Phys.](#)

- [Lett. B](#) **807** (2020) 135537 [[2003.02950](#)].
- [39] S.-Y. Guo and Z.-L. Han, Observable Signatures of Scotogenic Dirac Model, [JHEP](#) **12** (2020) 062 [[2005.08287](#)].
- [40] N. Bernal, J. Calle and D. Restrepo,
Anomaly-free Abelian gauge symmetries with Dirac scotogenic models, [Phys. Rev. D](#) **103** (2021) 095032 [[2102.06211](#)].
- [41] T. A. Chowdhury, M. Ehsanuzzaman and S. Saad,
Dark Matter and $(g - 2)_{\mu,e}$ in radiative Dirac neutrino mass models, [2203.14983](#).
- [42] D. Borah, E. Ma and D. Nanda,
Dark SU(2) gauge symmetry and scotogenic Dirac neutrinos, [Phys. Lett. B](#) **835** (2022) 137539 [[2204.13205](#)].
- [43] MEG collaboration,
Search for the lepton flavour violating decay $\mu^+ \rightarrow e^+ \gamma$ with the full dataset of the MEG experiment, [Eur. Phys. J. C](#) **76** (2016) 434 [[1605.05081](#)].
- [44] Y. Kuno and Y. Okada, Muon decay and physics beyond the standard model, [Rev. Mod. Phys.](#) **73** (2001) 151 [[hep-ph/9909265](#)].
- [45] MEG II collaboration, The design of the MEG II experiment, [Eur. Phys. J. C](#) **78** (2018) 380 [[1801.04688](#)].
- [46] M. E. Peskin and T. Takeuchi, A New constraint on a strongly interacting Higgs sector, [Phys. Rev. Lett.](#) **65** (1990) 964.
- [47] M. E. Peskin and T. Takeuchi, Estimation of oblique electroweak corrections, [Phys. Rev. D](#) **46** (1992) 381.
- [48] H. E. Haber and D. O’Neil,
Basis-independent methods for the two-Higgs-doublet model III: The CP-conserving limit, custodial symmetry, [Phys. Rev. D](#) **83** (2011) 055017 [[1011.6188](#)].
- [49] A. Beniwal, J. Herrero-García, N. Leerdam, M. White and A. G. Williams,
The ScotoSinglet Model: a scalar singlet extension of the Scotogenic Model, [JHEP](#) **21** (2020) 136 [[2010.05937](#)].
- [50] G. Passarino and M. J. G. Veltman,
One Loop Corrections for $e^+ e^-$ Annihilation Into $\mu^+ \mu^-$ in the Weinberg Model, [Nucl. Phys. B](#) **160** (1979) 151.

- [51] PARTICLE DATA GROUP collaboration, Review of Particle Physics, [PTEP **2022** \(2022\) 083C01](#).
- [52] E. Lundstrom, M. Gustafsson and J. Edsjo, The Inert Doublet Model and LEP II Limits, [Phys. Rev. D **79** \(2009\) 035013 \[0810.3924\]](#).
- [53] ATLAS collaboration,
Search for invisible Higgs-boson decays in events with vector-boson fusion signatures using 139 fb⁻¹ of proto
[2202.07953](#).
- [54] M. Gustafsson, S. Rydbeck, L. Lopez-Honorez and E. Lundstrom,
Status of the Inert Doublet Model and the Role of multileptons at the LHC, [Phys. Rev. **D86** \(2012\) 075019 \[1206.6316\]](#).
- [55] A. Datta, N. Ganguly, N. Khan and S. Rakshit,
Exploring collider signatures of the inert Higgs doublet model, [Phys. Rev. **D95** \(2017\) 015017 \[1610.00648\]](#).
- [56] P. Poulose, S. Sahoo and K. Sridhar,
Exploring the Inert Doublet Model through the dijet plus missing transverse energy channel at the LHC, [Phys. Lett. **B765** \(2017\) 300 \[1604.03045\]](#).
- [57] M. Hashemi and S. Najjari, Observability of Inert Scalars at the LHC, [1611.07827](#).
- [58] A. Belyaev, G. Cacciapaglia, I. P. Ivanov, F. Rojas and M. Thomas,
Anatomy of the Inert Two Higgs Doublet Model in the light of the LHC and non-LHC Dark Matter Searches
[1612.00511](#).
- [59] A. Belyaev, T. R. Fernandez Perez Tomei, P. G. Mercadante, C. S. Moon, S. Moretti, S. F. Novaes et al.,
Advancing LHC probes of dark matter from the inert two-Higgs-doublet model with the monojet signal, [Phys. Rev. D **99** \(2019\) 015011 \[1809.00933\]](#).
- [60] CMS collaboration,
Measurements of Higgs boson production cross sections and couplings in the diphoton decay channel at $\sqrt{s} =$
[JHEP **07** \(2021\) 027 \[2103.06956\]](#).
- [61] P. Gondolo, J. Hisano and K. Kadota,
The Effect of quark interactions on dark matter kinetic decoupling and the mass of the smallest dark halos, [Phys. Rev. D **86** \(2012\) 083523 \[1205.1914\]](#).
- [62] P. Gondolo and G. Gelmini, Cosmic abundances of stable particles: Improved analysis, [Nucl.](#)

- [Phys. B](#) **360** (1991) 145.
- [63] K. Griest and D. Seckel, Three exceptions in the calculation of relic abundances, [Phys. Rev. D](#) **43** (1991) 3191.
- [64] SPT-3G collaboration, Particle Physics with the Cosmic Microwave Background with SPT-3G, [J. Phys. Conf. Ser.](#) **1468** (2020) 012008 [[1911.08047](#)].
- [65] CMB-S4 collaboration, CMB-S4 Science Book, First Edition, [1610.02743](#).
- [66] G. Bélanger, F. Boudjema, A. Goudelis, A. Pukhov and B. Zaldivar, micrOMEGAs5.0 : Freeze-in, [Comput. Phys. Commun.](#) **231** (2018) 173 [[1801.03509](#)].
- [67] J. M. Cline, K. Kainulainen, P. Scott and C. Weniger, Update on scalar singlet dark matter, [Phys. Rev. D](#) **88** (2013) 055025 [[1306.4710](#)].
- [68] DARWIN collaboration, DARWIN: towards the ultimate dark matter detector, [JCAP](#) **11** (2016) 017 [[1606.07001](#)].